MODELING OF OPTICAL BEAM SPREAD IN SEA ICE

FINAL REPORT
May 1998

Curtis D. Mobley

Sequoia Scientific, Inc.
9725 S.E. 36th Street, Suite 308
Mercer Island, WA 98040

Prepared for the
Environmental Optics Program
Office of Naval Research
Contract Number: N00014-97-C-0023

SEQUOIA

REPORT DOCUMENTATION PAGE

Form Approved
OMB No. 0704-0188

1. AGENCY USE ONLY (Leave blank)	2. REPORT DATE	3. REPORT TYPE AND DATES COVERED
	May 1998	FINAL REPORT

4. TITLE AND SUBTITLE
Modeling of Optical Beam Spread in Sea Ice

5. FUNDING NUMBERS
N00014-97-C-0023

6. AUTHOR(S)
Curtis D. Mobley

7. PERFORMING ORGANIZATION NAME(S) AND ADDRESS(ES)
Sequoia Scientific, Inc.
9725 SE 36th Street, Suite 308
Mercer Island, WA 98040

8. PERFORMING ORGANIZATION REPORT NUMBER
Project 21 - Final

9. SPONSORING/MONITORING AGENCY NAME(S) AND ADDRESS(ES)
Environmental Optics Program, Code 3220P
Office of Naval Research
800 N. Quincy Street
Arlington, VA 22217-5660

10. SPONSORING/MONITORING AGENCY REPORT NUMBER

11. SUPPLEMENTARY NOTES
Includes copies of two papers submitted for publication

12a. DISTRIBUTION/AVAILABILITY STATEMENT
Distribution unlimited

12b. DISTRIBUTION CODE

13. ABSTRACT *(Maximum 200 words)*

This two-year theoretical investigation of the optical properties of first-year sea ice yielded several important results: (1) beam-spread-function measurements provide an important constraint on inversion of optical data to obtain ice scattering properties; (2) several hundred optical path lengths can be required to approach the asymptotic radiance distribution for point light sources, even though the ice is highly scattering; (3) photon diffusion theory gives a reasonably good description of light propagation deep within sea ice and, more importantly, shows that sea ice scattering phase functions are highly peaked near the forward scattering direction; (4) classical radiative transfer theory is adequate for prediction of light propagation within sea ice, and (5) it is possible to begin with sea ice physical properties and proceed in a rigorous fashion to predict sea ice inherent and apparent optical properties.

14. SUBJECT TERMS
Sea Ice, Radiative transfer, Optics, Hydrolight, Diffusion Theory

15. NUMBER OF PAGES
40

16. PRICE CODE

17. SECURITY CLASSIFICATION OF REPORT	18. SECURITY CLASSIFICATION OF THIS PAGE	19. SECURITY CLASSIFICATION OF ABSTRACT	20. LIMITATION OF ABSTRACT
UNCLASSIFIED	UNCLASSIFIED	UNCLASSIFIED	Unlimited

TABLE OF CONTENTS

MODELING OF OPTICAL BEAM SPREAD IN SEA ICE

FINAL REPORT

Curtis D. Mobley
Sequoia Scientific, Inc.
9725 S.E. 36th Street, Suite 308
Mercer Island, WA 98040
phone: 206-230-8166 x 109
fax: 206-230-8175
email: mobley@sequoiasci.com

ABSTRACT

This two-year theoretical investigation of the optical properties of first-year sea ice yielded several important results: (1) beam-spread-function measurements provide an important constraint on inversion of optical data to obtain ice scattering properties; (2) several hundred optical path lengths can be required to approach the asymptotic radiance distribution for point light sources, even though the ice is highly scattering; (3) photon diffusion theory gives a reasonably good description of light propagation deep within sea ice and, more importantly, shows that sea ice scattering phase functions are highly peaked near the forward scattering direction; (4) classical radiative transfer theory is adequate for prediction of light propagation within sea ice, and (5) it is possible to begin with sea ice physical properties and proceed in a rigorous fashion to predict sea ice inherent and apparent optical properties.

INTRODUCTION

The absorption properties of sea ice can be determined by measuring the absorption coefficient of the liquid water obtained from melted ice cores. However, the scattering properties of sea ice are determined by particle inclusions (brine pockets, air bubbles, biogenic and terrigenous particles) that must not be disturbed if an accurate measurement of the scattering properties is to be made. Even the simple act of removing an ice core may allow the brine channels to drain, for example, thus giving the ice core scattering properties much different from the parent ice. It is therefore particularly difficult to measure scattering coefficients and scattering phase functions in sea ice.

In separately funded work, R. Maffione devised an ingenious experiment in which the optical beam spread function (BSF) was measured between pairs of holes drilled in the ice (Maffione and Mobley, 1998). Such BSF data were taken during the ONR-Sponsored 1994 EMPOSI (ElectroMagnetic Properties Of Sea Ice) field experiment at Barrow, Alaska. This unique experiment gave the BSF along horizontal paths within the ice, as a function of depth within the ice and path length (distance between the holes). Working in conjunction with Maffione, I examined the extent to which such BSF data can be used to deduce the ice scattering properties.

In addition, I investigated how well classical radiative transfer theory (as opposed to a full electromagnetic treatment beginning with Maxwell's equations) can predict visible light propagation in sea ice, which sometimes violates the implicit assumptions underlying radiative transfer theory. That investigation was carried out in collaboration with several of the EMPOSI investigators, who made a variety of relevant optical and physical measurements during the 1994 field experiment.

APPROACH

Because sea ice is primarily a scattering (rather than an absorbing) medium, the BSF is particularly sensitive to the angular shape of the scattering phase function. Therefore, measured BSF data can be used as the basis for an implicit inverse model to deduce the ice phase function, which cannot be measured in situ. During the first year of this work, I developed a Monte Carlo code for predicting the BSF, given the absorbing and scattering properties of the ice. The details of this model are given in Mobley (1996). The inversion was then effected by varying the phase function in the Monte Carlo model until agreement between the predicted and measured BSFs was obtained. The absorption coefficient of the ice was known from independent measurements made (by G. Cota) during the field experiment. The inversion of the BSF data then gave the scattering coefficient and phase function that were consistent with the measured BSF.

The measured absorption and deduced scattering properties of the ice were then used as input to the Hydrolight radiative transfer numerical model (Mobley, 1994, 1995) to predict other optical quantities of interest, such as albedos, transmittances through the ice, and diffuse attenuation functions within the ice. Comparison of such predictions with observations made during the 1994 EMPOSI field experiment provided an important test of the applicability of radiative transfer theory to sea ice.

The utility of classical photon diffusion theory for modeling light propagation in sea ice was also examined by comparing results derived from diffusion theory with observation and with Hydrolight predictions.

RESULTS

Several major results were obtained from the modeling studies. First, inversion of the BSF data showed that within the interior of the ice (at Barrow site 2, May 1994, at a wavelength of 670 nm), a one-term Henyey-Greenstein (OTHG) scattering phase function with an asymmetry parameter of $g = 0.98$ is consistent with the BSF data; the scattering coefficient σ is approximately 200 m^{-1}. The measured absorption coefficient of $\kappa \approx 0.4$ m^{-1} then gives an albedo of single scattering of 0.998. These values are consistent with previous estimates for ice of the type found at Barrow (Perovich, 1996). Computations carried out (under separate funding) by T. Grenfell starting with measured ice physical properties (brine pocket and air bubble size distribution statistics) and using Mie scattering theory gave similar results for the ice scattering properties (see Mobley *et al.*, 1998; this paper is attached as Appendix A). Figure 1 shows the good agreement between predicted and measured BSFs.

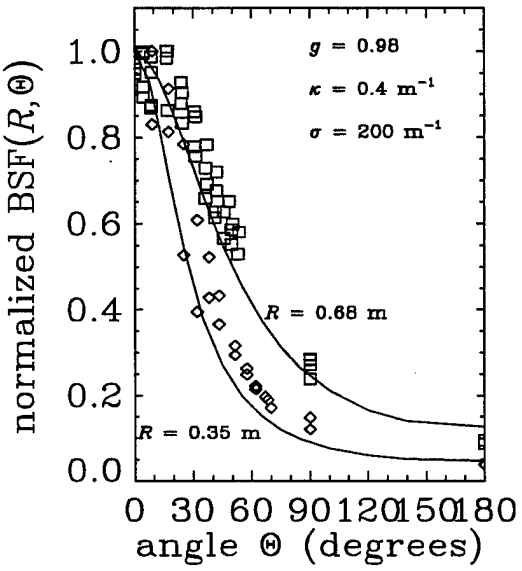

Fig. 1. Computed (lines) and measured (squares and diamonds) BSFs for path lengths (hole separations) of $R = 0.35$ and 0.68 m (from Mobley *et al.*, 1998). Note the good agreement even at 180 degrees, which is opposite the direction of the initial beam propagation.

Second, Monte Carlo modeling shows that the approach of the BSF to its asymptotic value is extremely slow, even though the ice is highly scattering. This is both because the BSF arises from a point light source and because the ice phase function is highly peaked in the forward direction. Figure 2 shows the dependence on optical distance τ from the light source of a diffuse attenuation function (K function) for the BSF; the K function is still 26% larger than its asymptotic value after 300 optical path lengths.

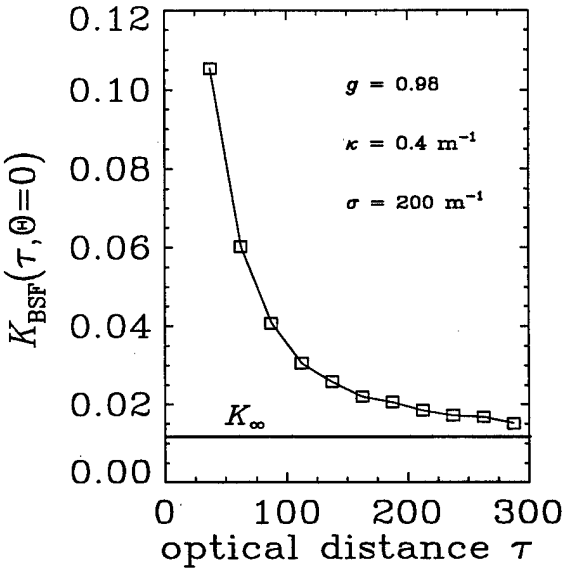

Fig 2. Approach of a diffuse attenuation coefficient for the BSF to its asymptotic value K_∞. For the ice being modeled, τ = 300 corresponds to a physical distance of 1.5 m.

Third, classical diffusion theory can be used with reasonable accuracy to model the propagation of sunlight within the interior of the ice (Mobley and Maffione, 1998; this paper is attached as Appendix B). Diffusion theory is valid in this situation because distributed light sources, such as sky light incident onto the air-ice surface, develop an asymptotic radiance distribution much faster (within a few tens of optical path lengths) than do point light sources. Figure 3 shows the agreement between K_d as predicted by an exact radiative transfer model (Hydrolight) and the K value given by diffusion theory. Moreover, diffusion theory provides an important constraint on the possible values of the ice scattering properties (Mobley and Maffione, 1998)

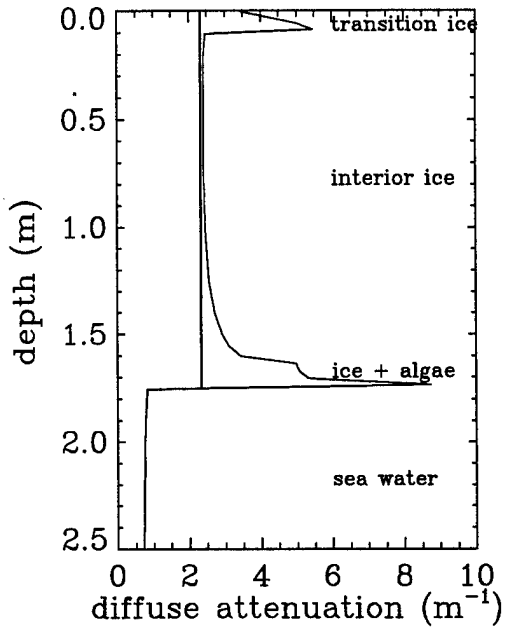

Fig. 3. Comparison of diffusion theory (dotted line) and exact radiative transfer theory (solid line) in the interior of the ice, which was modeled as a four-layer system (Mobley *et al.*, 1998). Note that diffusion theory is not valid near the air-ice (at depth 0) and ice-water (at depth 1.74 m) boundaries.

Finally, Mobley *et al.* (1998) showed that it is possible to (1) start with sea ice physical properties (such as brine pocket and bubble size distributions), (2) predict the ice scattering properties (using modified Mie scattering theory with the physical properties as input), and then (3) use the predicted scattering properties (along with known absorption properties) as input to radiative transfer models such as Hydrolight to accurately predict various optical properties (such as albedos, transmittances, and diffuse attenuation). The good agreement between measured data and various radiative transfer predictions as seen in Mobley *et al.*, (1998) shows that classical radiative transfer theory adequately describes visible light propagation in sea ice.

LONG-TERM IMPACT

Light absorption and scattering in sea ice play a central role in ice thermodynamics, in biological productivity below the ice, and in some remote sensing. Obtaining a self-consistent set of inherent optical properties of sea ice – in particular the scattering phase function – opens the door to the extensive use of radiative transfer theory for solving problems related to light transfer in sea ice. Moreover, the Monte Carlo BSF model developed here, which is quite general and also can compute point spread functions, already has been used for modeling underwater point spread functions. This model can address many problems associated with underwater imaging systems.

REFERENCES

Maffione, R. A. and C. D. Mobley, 1998. Theory and measurements of the complete beam spread function of sea ice. *Limnol. Oceanogr.*, in press.

Mobley, C. D., 1994. *Light and Water: Radiative Transfer Theory in Natural Waters.* Academic Press, 592 pages.

Mobley, C. D., 1995. Hydrolight 3.0 Users' Guide. Final Report, SRI Project 5632, SRI International, Menlo Park, CA, 65 pages.

Mobley, C. D., 1996. Monte Carlo simulation of a point light source in an infinite medium. SRI Technical Report, Project 7311, May 1996, 39 pages.

Mobley, C. D. and R. A. Maffione, 1998. The utility of first-order diffusion theory for modeling light propagation in sea ice. *J. Geophys. Res.*, in review. Attached as Appendix B.

Mobley, C. D., G. Cota, T. C. Grenfell, R. A. Maffione, W. S. Pegau, and D. K. Perovich, 1998. Modeling light propagation in sea ice. *IEEE Trans. Geosci. and Rem. Sens.*, in review. Attached as Appendix A.

Perovich, D. K., 1996. The optical properties of sea ice. Monograph 96-1, U. S. Army cold Reg. Res. Engin. Lab., Hanover, NH, 25 pages.

APPENDIX A

Reference: Mobley *et al.* (1998)

This paper is in review by *Transactions of Geoscience and Remote Sensing*
(special edition on the EMPOSI Program)
at the time of preparation of this contract Final Report

Modeling Light Propagation in Sea Ice

Curtis D. Mobley
Sequoia Scientific, Inc.
9725 SE 36th St. Suite 308
Mercer Island, WA 98040

Glenn F. Cota
Center for Coastal Physical Oceanography
768 West 52nd St.
Old Dominion University
Norfolk, VA 23508

Thomas C. Grenfell
Department of Atmospheric Sciences
Box 351640
University of Washington
Seattle, WA 98195

Robert A. Maffione
Hydro-Optics, Biology, and Instrumentation Laboratories
55 Penny Lane, Suite 104
Watsonville, CA 95076

W. Scott Pegau
College of Oceanographic and Atmospheric Science
Oregon State University
Ocean Administration Building 104
Corvallis, OR 97331

Donald K. Perovich
U.S. Army Cold Regions Research and Engineering Laboratory
72 Lyme Road
Hanover, NH 03755

Abstract

This paper outlines the process by which it is possible to begin with the physical properties of sea ice (such as the size distributions of brine pockets and air bubbles), and then to predict the optical absorption and scattering properties of the ice, and finally to use these inherent optical properties in radiative transfer models to predict light propagation within the ice. Each step of this entire process is illustrated by application to a comprehensive data set of sea ice physical and optical properties. Good agreement is found between measured and modeled beam spread functions, albedos, and transmittances.

I. INTRODUCTION

The 1994 EMPOSI (Electromagnetic Properties of Sea Ice) field experiment near Barrow, Alaska, yielded a unique data set of ice physical, electromagnetic, and optical properties [1]. Experiment Site 2 was located approximately 200 m offshore in the Beaufort Sea on shorefast, first-year ice approximately 1.7 m thick. The physical, electromagnetic, and optical properties of this ice are described in [2] and [3].

This paper illustrates how we can start with the ice physical properties and predict the optical absorption and scattering properties of the ice, and in turn use these optical properties in radiative transfer models to predict light propagation within the ice. For brevity, we discuss only one ice sample from the Site 2 dataset, and one wavelength. The application of the methods presented here to the more extensive analysis of other data and other wavelengths is reserved for the authors' individual papers.

The various measurements made at Site 2 and used in this paper were made within a few tens of meters of each other in horizontal location and at various times on May 5-7, 1994. Thus the data are not strictly co-located and simultaneous, and it is implicitly assumed in our analysis that the ice is horizontally homogeneous over the measurement site and temporally stable over the three-day period.

We selected a mid-ice depth of approximately 0.5 m for detailed modeling because the ice physical properties were fairly constant with depth in this region and because optical beam spread measurements were available over horizontal paths at that depth. Likewise, a wavelength of 670 nm was selected because that was the wavelength of the laser used in the horizontal beam spread measurements.

II. THE DATA SET

Selected values of temperature, salinity, density, and brine pocket volume at Site 2 [2] are shown for reference in Table I. The brine pockets had size distributions that are well described by lognormal distributions for the cross sectional areas (in a horizontal plane) of the brine pockets. The parameters of the distributions are given in Table 1 of [2], and the distributions are plotted in Figure 7 of [2]. These data are the foundation for our predictions of ice optical properties.

Optical measurements made at Site 2 included the spectral absorption coefficient of dissolved and particulate matter as a function of depth within the ice, spectral albedo of and transmittance through both snow-covered and bare ice, spectral diffuse attenuation as a function of depth within the ice, beam spread functions (BSFs) along horizontal paths at selected depths and path distances within the ice, and BSFs along vertical paths through the ice [3]. A small subset of these measurements, as needed for the discussion below, is given in Table I.

The spectral absorption coefficient for particulate material within the ice was measured on melted ice core by collecting the particulates on Whatman GF/F glass fiber filters and measuring the absorption in a dual-beam scanning spectrophotometer [4]. The absorption by dissolved matter was determined from the filtrate [5].

The spectral albedo was determined by measuring the downwelling and upwelling plane irradiances just above the ice surface. Spectral transmittance through the ice was determined using an upward-looking fiber-optic sensor on an L-shaped arm deployed through a hole in the ice.

Diffuse attenuation within the ice was measured with a 13 cm diameter diffusing sphere enclosed between light shields above and below the sphere. This assembly was designed for insertion into the holes used in making the horizontal BSF measurements. This instrument measured an azimuthally averaged irradiance that is weighted towards approximately horizontal directions. The rate of change with depth of this irradiance then yields a diffuse attenuation coefficient K_{sphere} that is particular to the geometry of the collector. However, for sufficient depths within the ice, all diffuse attenuation coefficients approach the same asymptotic value K_{∞}, and K_{sphere} should then be comparable to any other K function.

The beam spread function is defined [6] as the irradiance distribution at distance R and angle Θ generated by a narrow collimated beam located at $R = 0$ and emitting light in the $\Theta = 0$ direction, normalized by the power of the light source. The irradiance is measured on a surface normal to the radial distance R. Figure 1 shows BSF data taken along horizontal paths within the ice. The BSF was measured by drilling two vertical holes a distance R apart

in the ice. A pulsed, collimated laser light source was placed in one hole and a cosine irradiance detector in the other, both at the same depth. The BSF was then measured through a full 360 degrees in Θ by rotating the source while holding the detector fixed. Phase synchronous detection was used so that the ambient light field within the ice could be subtracted out. The details of these measurements are given in [7]. In the present paper we use only a small part of the entire BSF data set, namely the BSFs at one depth, 0.45 m, for two hole separations, $R = 0.35$ and 0.68 m. To the extent that the ice is isotropic, the BSF is symmetric about $\Theta = 0$. Therefore, for viewing convenience in Figure 1, we have plotted the BSF for $-180° \le \Theta \le 0°$ onto the angle range from $0° \le \Theta \le 180°$. The data for $R = 0.68$ m include measurements made for holes both perpendicular and parallel to the ice c axis; the data for $R = 0.35$ m are for holes parallel to the c axis. More extensive presentations of BSF data are given in [3] and [7].

III. Predicting Inherent Optical Properties

Brine pockets in sea ice are usually vertically oriented, irregularly shaped channels of varying lengths. Little statistical data are available on the three-dimensional structure of brine pockets; and even if such data were available, calculations of light scattering by anisotropic, oriented brine pockets would be exceedingly difficult. On the other hand, photomicrographs of ice horizontal thin sections show [2] that the cross-sectional areas A of the brine pockets are well described by a lognormal probability distribution function (PDF):

$$\mathrm{PDF}(A) = \frac{1}{\sqrt{2\pi s_A^{\,2}}}\,\frac{1}{A}\exp\left[-\frac{(\ln A - \ln A_m)^2}{2s_A^{\,2}}\right]. \qquad (1)$$

If the area A is measured in square millimeters, then the median area A_m and standard deviation s_A of $\ln A$ for the ice at a depth of 0.75 m at Site 2 are $A_m = 0.013$ mm^2 and $s_A = 1.01$. These values of A_m and s_A correspond to a mean brine pocket area of $A_m \exp(s_A^2/2) = 0.023$ mm^2 (see Table 1, "first-year ice" in [2]).

In order to capitalize on these brine pocket statistics and in order to simplify the scattering calculations, a simple model of scattering by brine pockets was used. It was first assumed that the brine pockets can be modeled as vertically oriented prolate spheroids with a 5:1 ratio of major:minor axes. The median and standard deviation of the cross-sectional areas were then used to determine the corresponding statistics of the minor axes of the prolate spheroids. The prolate spheroids were then converted to equivalent spheres having the same volume-to-surface-area as the prolate spheroids. The results are that the median equivalent-sphere radius of a brine pocket is $r_{bp} = 0.16$ mm and the corresponding standard deviation s_{bp}

is 0.51. Under the further assumption that these brine pocket equivalent-sphere radii also obey a lognormal size distribution, the A_m and s_A parameters of the area PDF can be replaced by the corresponding parameters r_{bp} and s_{bp} of the radius PDF. These equivalent spheres have the same brine volume of 5.5% as was observed.

Air bubbles were assumed to be spherical and lognormally distributed in size. Measured values for air bubbles in pancake ice (not measured at Site 2; see Table 1, "pancakes" in [2]) were assumed to be representative of the particular ice being modeled. The resulting lognormal parameters for the bubble distribution are $r_{bub} = 0.20$ mm and $s_{bub} = 0.62$.

The lognormal size distributions for brine pocket and air bubble radii were used as input to Mie scattering calculations of the optical absorption and scattering efficiencies and mean cosines of the scattering angle due to brine pockets and air bubbles. These calculations were performed in 15 bins logarithmically spaced between $s/3$ and $3s$ for each lognormal distribution. The complex indices of refraction, n = (real part, imaginary part), for pure ice and brine at 670 nm are respectively ($1.307, 2.02\times10^{-8}$) [8], [9] and ($1.355, 2.10\times10^{-8}$) [10], [11]. The indices of refraction of the brine pockets and air bubbles relative to the ice itself, as used in the Mie calculations, are therefore n_{br} = ($1.037, 4.45\times10^{-11}$) and n_{air} = ($0.7651, -1.18\times10^{-8}$).

The absorption efficiencies Q^{abs} obtained from the Mie calculations are finally used with the particle size distributions $N(r)$ to compute the total absorption coefficient κ_{tot} of the ice-brine-bubble system:

$$\begin{aligned} \kappa_{tot} &= \kappa_{ice} + \kappa_{br} + \kappa_{bub} \\ &= \kappa_{ice} + \int Q_{br}^{abs}(r_{br})\, \pi r_{br}^2\, N_{br}(r_{br})\, dr_{br} + \int Q_{bub}^{abs}(r_{bub})\, \pi r_{bub}^2\, N_{bub}(r_{bub})\, dr_{bub} . \end{aligned} \tag{2}$$

A corresponding equation using the scattering efficiencies gives the total scattering coefficient σ_{tot}; the pure ice itself was assumed to have negligible scattering at this wavelength. The effective mean cosine of the scattering angle is computed from

$$g = \frac{g_{br}\,\sigma_{br} + g_{bub}\,\sigma_{bub}}{\sigma_{br} + \sigma_{bub}} . \tag{3}$$

Because of the uncertainties about the brine pocket model and some of the input (such as the actual bubble concentration and size distribution), Mie calculations were performed for a range of possible conditions at Site 2. These calculations show that the total absorption given by Eq. 2 is approximately 0.38 m^{-1}; this value is determined primarily by the ice itself. The total scattering coefficient varies considerably with the details of the brine pocket and bubble concentrations and size distributions; the range of predicted values for Site 2 is from

175 (few bubbles) to 250 m^{-1} (many bubbles), with a likely value of around 200 m^{-1}. This σ range is consistent with previous studies [12]. Most of the scattering is due to the brine pockets, and most of the variability in the total is due to the bubbles. At the temperature of the Site 2 ice, the brine pockets contain no precipitated salts, which can greatly increase the scattering if present.

The Mie calculations did not include the effects of mineral or biological particles that were imbedded in the ice. Measurement of the spectral absorption of these imbedded particles shows that they contributed at most 0.02 m^{-1} to the absorption at 670 nm. Therefore, in the modeling below, we take the total absorption at 670 nm to be $\kappa_{tot} = 0.38 + 0.02 = 0.40\ m^{-1}$. Imbedded particles likely contribute much less to the total scattering than the brine pockets and bubbles; we therefore keep the total scattering at $\sigma_{tot} = 200\ m^{-1}$.

The predicted mean cosine of the scattering angle for the brine pockets is $g_{br} = 0.99$. Such a large value occurs because the brine pockets are much larger than the wavelength of the light and their index of refraction closely matches that of the ice, so that scattering is predominately by diffraction. The bubbles have $g_{bub} = 0.86$. Even though the bubbles are somewhat larger than the brine pockets, their g value is smaller because the large index of refraction difference between the ice and air gives greater scattering at large angles. The effective g value given by Eq. 3 ranges from 0.96 (many bubbles) to 0.99 (few bubbles), with a likely value of around 0.98.

We assume that the scattering phase function $\tilde{\beta}(\psi)$ of the sea ice can be described by a one-term Henyey-Greenstein (OTHG) phase function:

$$\tilde{\beta}(\psi) = \frac{1}{4\pi} \frac{1 - g^2}{(1 + g^2 - 2g\cos\psi)^{3/2}}. \tag{4}$$

Here ψ is the scattering angle, and $g = 0.98$ is the average of $\cos\psi$ when weighted by $\tilde{\beta}(\psi)$ and integrated over all scattering directions. The inherent optical properties (IOPs) κ, σ, and $\tilde{\beta}(\psi)$ give us the information necessary for the prediction of any lightfield quantity, after imposition of appropriate boundary conditions.

IV. Prediction of Beam Spread Functions

A first test of the correctness of the predicted inherent optical properties of the ice can be made by using the IOPs to predict the BSF. Prediction of the BSF provides a particularly stringent test of the IOPs because an entire function — the shape of the BSF — must be predicted, not just a single number as is the case, for example, with a prediction of albedo or transmission. The Θ dependence of the BSF is strongly dependent on the ψ dependence of

the scattering phase function.

A Monte Carlo ray-tracing model for the simulation of point light sources in an infinite, homogeneous medium [13] was used to predict the BSFs corresponding to the measured data seen in Fig. 1. The predictions are shown as the solid lines in Fig. 1. The agreement is quite good considering the remaining uncertainties in the IOPs (in particular, the actual shape of the phase function) and the possible effects of inhomogenities in the ice.

V. Prediction of Daylight Propagation

We next model the interaction of daylight with the entire ice sheet. A number of radiative transfer models are capable of simulating daylight propagation in an atmosphere-ice-water system [14]-[16]. The model we use here is the Hydrolight radiative transfer model [16], [17]. Hydrolight solves the radiative transfer equation from first principles using invariant imbedding methods to obtain the spectral radiance distribution as a function of depth, direction, and wavelength throughout and leaving the medium. The model can accept as input any depth profile of IOPs and any incident sky radiance distribution. Both rough and smooth sea or ice surfaces can be simulated. Quantities such as irradiances, albedos, or diffuse attenuation functions are obtained from their definitions after the radiance distribution is computed. In order to employ this or any other such model, we must first specify appropriate IOPs and boundary conditions for the system.

The IOPs predicted by the Mie calculations and used above for the beam spread modeling apply only to the interior region of the ice sheet. Although some banding could be seen in ice cores, indicating at least some variability with depth in the IOPs, measured temperature, salinity, and density profiles (Fig. 5 in [2]) are fairly constant throughout the interior of the ice sheet. Moreover, the Mie calculations were based on parameter values taken from the midrange of values found within the ice interior. We therefore assume that the IOPs computed above are valid for the interior of the ice, namely from a depth of 0.1 to 1.6 m. However, very near the ice surface and bottom there were thin layers that differed considerably from the ice interior in their optical properties. These IOPs of these layers should be modeled separately, even if approximately.

Near the ice surface, there was a 0.1 m thick layer of fine-grained transition ice that had an air content of 3.9-4.1%, in contrast to values between 0.5 and 1% (averaging about 0.8%) within the interior of the ice sheet. This transition layer likely will have a higher scattering coefficient σ and lower g because of the higher number of bubbles. We did not perform Mie calculations for this layer. However, simply assuming that the contribution by bubbles to the total scattering increases by a factor of 4.0%/0.8% = 5 over the contribution by bubbles deeper within the ice gives $\sigma = 250\ m^{-1}$ within the transition layer. Equation 3 yields

$g = 0.95$. The absorption, which is due primarily to the ice, is kept at $\kappa = 0.4$ m^{-1}.

The bottom surface of the ice contained a dense algae mat approximately 1 cm thick, with some algae distributed throughout the bottom few centimeters of the ice. The absorption coefficient due to algae and dissolved matter as measured on the bottom 13 cm of an ice core (from depth 1.61 m to 1.74 m) averaged 0.90 m^{-1}. Adding this value to the absorption by the ice itself, 0.38 m^{-1}, gives a total average absorption of $\kappa = 1.28$ m^{-1} with in the layer. The increase in scattering due to the algae was not measured, but is likely small compared to the scattering caused by the brine pockets and air bubbles; we therefore keep $\sigma = 200$ m^{-1} in this layer. Since the actual profile of absorption within this layer was not measured, we model the algae effects simply as a homogeneous layer between 1.61 and 1.74 m having the average κ and assumed σ values; the value of g is kept at 0.98.

The IOPs of the water below the ice were not measured. We therefore use $\kappa = 0.5$ m^{-1} and $\sigma = 0.1$ m^{-1}, along with a typical seawater phase function (Table 3.10, column 6, of [17]), as reasonable estimates of the water IOPs. The water below the ice was taken to be optically infinitely deep.

We now have in hand a simple, four-layer IOP model of the ice-algae-water system, which is summarized in Table II. The air-ice surface was taken to be somewhat rough via the artifice of using Cox-Munk capillary wave slope statistics for a wind speed of 15 m s^{-1} to model the radiance reflection and transmission properties of the ice surface. The sky was assumed to have a cardioidal radiance distribution, which is typical of a heavily overcast day. These surface boundary conditions give us the remaining information needed to run Hydrolight.

Hydrolight was run with the IOPs and boundary conditions just specified. The albedo of the ice-water system, the irradiance transmission through the ice, and the diffuse attenuation profile K_d within the ice were computed from the radiance distribution for comparison with measured values. The albedo is given by $A = E_u(\text{air})/E_d(\text{air})$, where $E_u(\text{air})$ and $E_d(\text{air})$ are respectively the upwelling and downwelling plane irradiances measured or computed just above the ice surface. The value measured in the field was $A = 0.48$; the value predicted by Hydrolight was 0.44. The transmission through the ice is $T = E_d(\text{water})/E_d(\text{air})$, where $E_d(\text{water})$ is measured or computed just below the bottom of the ice. In the present simulation, the computed value of E_d at $z = 1.75$ m was used. The measured T was 0.01; the predicted value was 0.0094. For both A and T, the measured and predicted values agree to within 8%, which is good agreement considering the crudeness of the IOP model. If the entire 1.74 m ice layer is modeled with the IOPs of the interior ice, the albedo decreases to 0.34 and the transmission increases to 0.015; these larger disagreements with observation highlight the importance that even relatively thin layers can have on optical propagation, if the layers have IOPs that are significantly different from the main body of the ice.

The solid line in Fig. 2 shows the depth profile of the diffuse attenuation function for downwelling plane irradiance,

$$K_d(z) = -\frac{1}{E_d(z)} \frac{dE_d(z)}{dz}. \tag{6}$$

It should be noted that although we are using four homogeneous layers to model the IOPs, Hydrolight can compute depth profiles of the radiance distribution and derived quantities with any desired depth resolution; its output is not simply layer-averaged values. The K_d profile shown in Fig. 2 was computed using $\Delta z = 0.01$ m in a finite-difference approximation of Eq. 6. This is much higher resolution than can be realized in the field, where a Δz of 0.1 m or greater is typical. Using a larger Δz smooths out the spikes in K_d that occur at the boundaries between layers with greatly different IOPs. The dashed line in Fig. 2 shows the diffuse attenuation K_{sphere} measured by the 13 cm diameter diffusing sphere described in the data section. The values of K_{sphere} would not be equal to K_d near a boundary because the instrument geometries are different. However, when optically far away from boundaries, these two K functions should both nearly equal the asymptotic value K_∞, which is 2.4 m^{-1} for the IOPs of the interior ice. (K_∞ was computed using an eigenmatrix method described in Section 9.6 of [17]) The value of K_d agrees well with K_∞ in the middle of the ice layer, indicating that the light field is nearly asymptotic. However, K_{sphere} averages about 0.7 m^{-1} at depths from 0.5 to 0.9 m, considerably less than the anticipated value of 2.4 m^{-1}. The reason for this discrepancy is not known. However, the measured K_{sphere} would be less than its true value if sky light were able to enter the hole into which the instrument was inserted and then to scatter through the ice and around the light baffles, which were intended to shield the diffusing sphere from the ambient light in the hole above it. We note that the average K_d value for the entire 1.74 m ice layer corresponding to the measured irradiance transmission of 0.01 is 2.6 m^{-1}. This value is consistent with the detailed K_d profile seen in Fig. 2. K values in the range of 2-4 m^{-1} are typical of young white ice [11], [18].

VI. Diffusion Theory

Several recent studies [7], [19], [20] have pointed out the utility of diffusion theory for modeling some aspects of light propagation in sea ice. According to diffusion theory, all light-field quantities decay with depth at a rate given by

$$K_{diff} = (\kappa + \sigma)\sqrt{3\,[1 - \omega_o - g\omega_o(1 - \omega_o)]} \tag{7}$$

Inserting the predicted IOPs for the interior of the ice into Eq. 7 gives $K_{diff} = 2.3$ m^{-1}. This

good agreement with the value of $K_\infty = 2.4\ m^{-1}$ just discussed indicates that diffusion theory is probably adequate for modeling daylight propagation in the interior of the ice. However, diffusion theory is valid only when optically far from boundaries. Note in Fig. 2 that even when Eq. 7 is evaluated with the IOPs of the transition and algae layers, K_{diff} differs considerably from K_d near the air-ice and ice-water boundaries. Diffusion theory therefore cannot be expected to adequately model the albedo of the ice, for example, which is largely determined by light scattering near the air-ice surface.

VII. Conclusions

The generally good agreements between predictions and observations obtained in this exercise indicate that the modeling tools now available are capable of predicting light propagation in sea ice with considerable accuracy. In particular, we have shown that it is possible to begin with the physical properties of sea ice and to carry through to the prediction of various optical quantities of interest in remote sensing, ice thermodynamics, and biological productivity. Any doubts about this process arising from philosophical concerns about the applicability of Mie theory to non-spherical brine pockets, or about the applicability of classical radiative transfer theory to light propagation in sea ice, appear to be unfounded.

Given our confidence in these forward models, we also can employ them as the core of implicit inverse models. Such models attempt to extract information about the ice IOPs from measured lightfield quantities by solving a sequence of forward problems as the input IOPs are varied and the model predictions are compared with observation. We do note, however, that it is important to have the largest possible suite of lightfield measurements when attempting such inversions. It is possible, for example, to obtain IOPs that correctly predict the albedo and transmittance, but which fail to predict the shape of the BSF, or vice versa. The EMPOSI field experiment showed that it is possible to obtain a comprehensive optical data set, which can greatly constrain the possible solutions of such inversions.

Acknowledgments

All authors wish to acknowledge the support of the Environmental Optics Program of the of the U. S. Office of Naval Research for support under the EMPOSI program; author T.C.G. also thanks the Remote Sensing Program for support.

TABLE I

SUMMARY OF MEASURED PHYSICAL AND OPTICAL PROPERTIES IN THE ICE INTERIOR.

Property	Value
Temperature	-5.7 deg C
Salinity	5.2‰
Density	0.92 gm cm^{-3}
Brine volume	5.5%
Air volume	< 1%
Absorption coefficient at 670 nm for dissolved and particulate matter	0.02 m^{-1}
Albedo at 670 nm, for bare ice	0.48
Transmittance at 670 nm, for bare ice	0.01
Diffuse "sphere" attenuation at 670 nm	0.7 m^{-1}
Horizontal BSF at 670 nm	see Fig. 1

TABLE II

FOUR-LAYER MODEL OF THE ICE-ALGAE-WATER SYSTEM AS USED TO MODEL DAYLIGHT INTERACTIONS WITH THE SYSTEM

depth z below ice surface (m)	description	κ (m^{-1})	σ (m^{-1})	phase function
$0 \le z < 0.1$	transition ice	0.4	250	OTHG, $g = 0.95$
$0.1 \le z < 1.61$	interior ice	0.4	200	OTHG, $g = 0.98$
$1.61 \le z < 1.74$	ice + algae	1.28	200	OTHG, $g = 0.98$
$1.74 \le z < \infty$	sea water	0.5	0.1	average seawater

REFERENCES

[1] K. Jezek, K. Golden, and D. K. Perovich, "Electromagnetic Properties of Sea Ice — ARI Overview," *IEEE Trans. Geosci. Rem. Sens.*, this issue.

[2] D. K. Perovich and A. J. Gow. "A quantitative description of sea ice inclusions," *J. Geophys. Res.*, vol. 101, no. (C8), pp. 18,327-18,343, 1996.

[3] D. K. Perovich, et al. "Field observations of the electromagnetic properties of first-year sea ice," *IEEE Trans. Geosci. Rem. Sens.*, this issue.

[4] B. G. Mitchell, "Algorithms for determining the absorption coefficient of aquatic particulates using the quantitative filter technique (QFT)," *Ocean Optics X*, R. W. Spinrad, editor, Proc. SPIE vol. 1302, pp 137-148, 1990.

[5] A. Bricaud, A. Morel and L. Prieur, "Absorption by dissolved organic matter of the sea (yellow substance) in the UV and visible domains," *Limnol. Oceanogr.*, vol. 26, no. 1, pp 43-53, 1981.

[6] L. E. Mertens and F. S. Replogle, Jr., "Use of point and beam spread functions for analysis of imaging systems in water," *J. Opt. Soc. Am.*, vol. 67, no. 8, pp. 1105-1117, 1977.

[7] R. A. Maffione and C. D. Mobley, "Theory and measurements of the complete beam spread function of sea ice," *Limnol. Oceanogr.*, in press, 1997.

[8] T. C. Grenfell and D. K. Perovich, "Radiation absorption coefficients of polycrystalline ice from 400 nm to 1400 nm," *J. Geophys. Res.*, vol. 86, no. C8, pp. 7447-7450, 1981.

[9] S. G. Warren, "Optical constants of ice from the ultraviolet to the microwave," *Appl. Optics*, vol. 23, pp. 1206-1225, 1984.

[10] G. A. Maykut and B. Light, "Refractive-index measurements of freezing sea-ice and sodium chloride brines," *Appl. Optics*, vol. 34, pp 950-961, 1995.

[11] T. C. Grenfell, "A theoretical model of the optical properties of sea ice in the visible and near infrared," *J. Geophys. Res.*, vol. 88, no. C14, pp. 9723-9735, 1983.

[12] D. K. Perovich, "The optical properties of sea ice," Monograph 96-1, U. S. Army Cold Reg. Res. Engin. Lab., Hanover, NH, 25 pp., 1996.

[13] C. D. Mobley, "Monte Carlo simulation of a point light source in an infinite medium," Technical Report, SRI Project 7311, SRI International, Menlo Park, CA, 39 pp, 1996.

[14] Z. Jin, K. Stamnes, W. F. Weeks, and S.-C. Tsay, "The effect of sea ice on the solar energy budget in the atmosphere-sea ice-ocean system: A model study," *J. Geophys. Res.*, vol. 99, no. C12, pp. 25,281-25,294, 1994.

[15] T. C. Grenfell, "A radiative transfer model for sea ice with vertical structure variations," *J. Geophys. Res.*, vol. 96, no. C9, pp. 16,991-17,001, 1991.

[16] C. D. Mobley, B. Gentili, H. R. Gordon, Z. Jin, G. W. Kattawar, A. Morel, P. Reinersman, K. Stamnes, and R. H. Stavn. "Comparison of numerical models for computing underwater light fields," *Appl. Optics*, vol. 32, no. 36, pp. 7484-7504, 1993.

[17] C. D. Mobley, *Light and Water: Radiative Transfer in Natural Waters*. San Diego, Academic Press, 1994.

[18] T. C. Grenfell and G. A. Maykut, "The optical properties of ice and snow in the Arctic basin," *J. Glaciol.*, vol. 18, no. 80, pp. 445-463, 1977.

[19] C. D. Mobley and R. A. Maffione, "Effects of absorption and boundary conditions on the utility of diffusion theory," *Ocean Optics XIII*, S. G. Ackleson and R. Frouin, editors, Proc. SPIE vol. 1963, pp 16-20, 1997.

[20] R. A. Maffione, "Theoretical developments on the optical properties of highly turbid waters and sea ice," *Limnol. Oceanogr.*, in press, 1997.

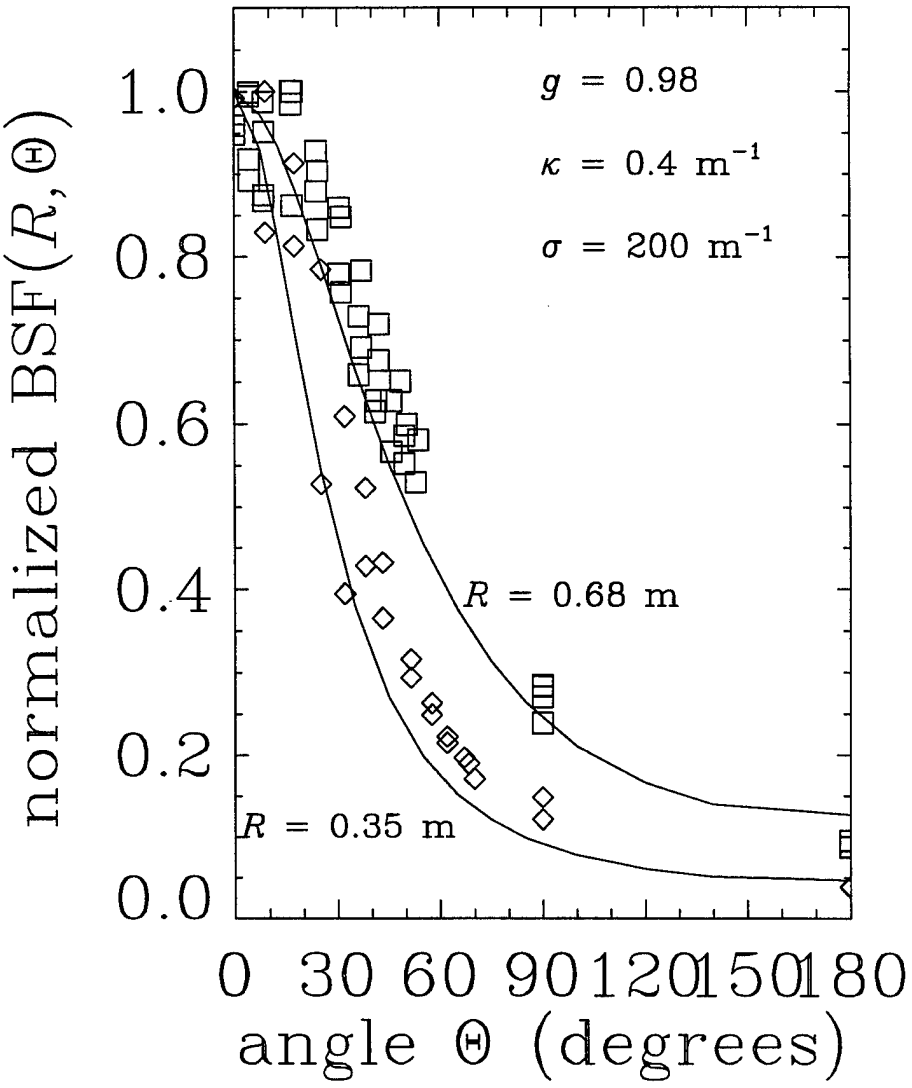

Fig. 1. Beam spread functions. The diamonds are measurements made with a hole separation (path length) of 0.35 m, and the squares are for 0.68 m. The solid lines are the BSFs predicted by the Monte Carlo model; note the good agreement even at 180 degrees.

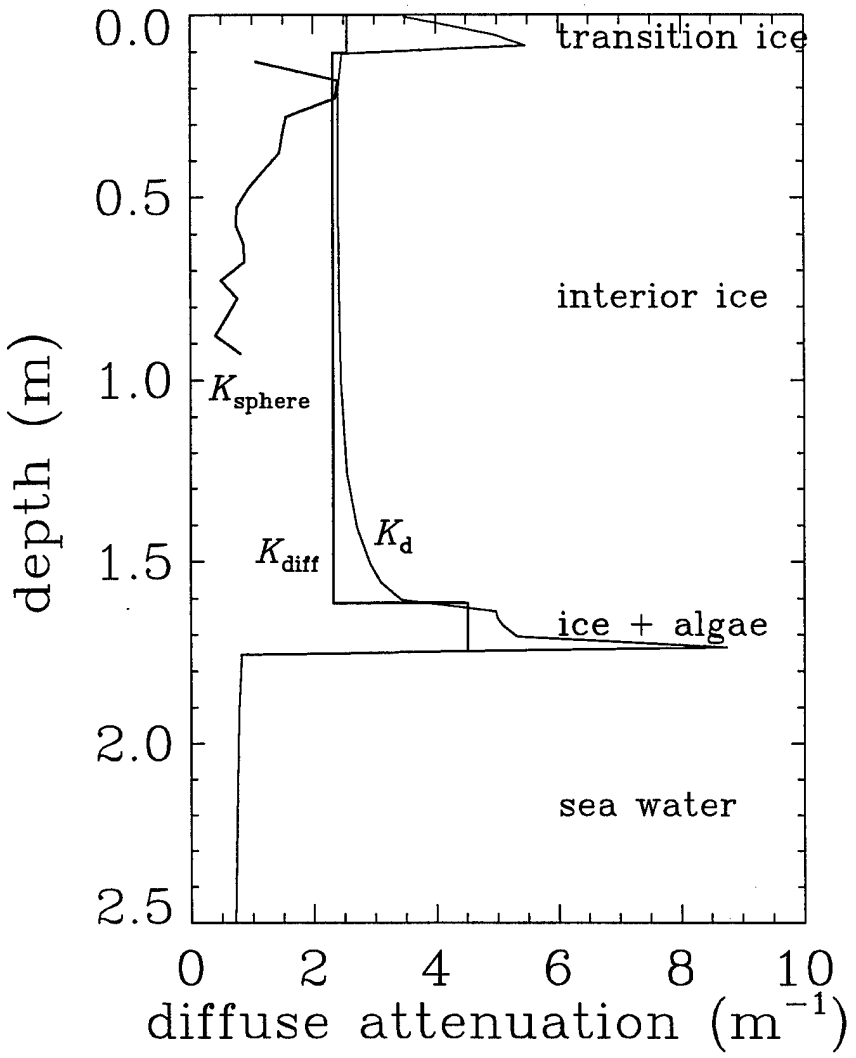

Fig. 2. Depth profiles of diffuse attenuation functions. The solid line is K_d as computed by Hydrolight using the IOPs of Table 2. The dashed line is the measured K_{sphere}. The dash-dot-dot line is K as given by diffusion theory (Eq. 7) for the IOPs of the ice

APPENDIX B

Reference: Mobley and Maffione (1998)

This paper is in review by the *Journal of Geophysical Research - Oceans* at the time of preparation of this contract Final Report

The Utility of First-order Diffusion Theory for Modeling Light Propagation in Sea Ice

Curtis D. Mobley
Sequoia Scientific, Inc.
9725 S.E. 36th St. Suite 308
Mercer Island, WA 98040

Robert A. Maffione
Hydro-Optics, Biology and Instrumentation Laboratories, Inc.
55 Penny Lane, Suite 104
Watsonville, CA 95076

Abstract

Numerical simulations show that first-order photon diffusion theory gives reasonably accurate predictions of light propagation deep in the interior of thick sea ice layers. Diffusion theory shows that the average cosine g of the scattering angle in sea ice must be very near one; this conclusion supports independent calculations based on Mie theory. These large g values give rise to optical boundary layers at the air-ice and ice-water boundaries that are tens of optical depths thick. Because of these boundary layers, diffusion theory cannot be used for computing the reflectance of ice sheets or the propagation of light through ice sheets. Although diffusion theory gives valuable information about the scattering properties of sea ice, it is too restrictive to be used as a framework for the simultaneous determination of both g and the scattering coefficient. The angular radiance distribution exiting the ice into the water is well approximated by a cardioidal distribution, although the same is not true for the radiance exiting the ice into the atmosphere.

1. Introduction

In addition to its origins in astrophysics [Eddington, 1916] and neutron transport calculations [Davison and Sykes, 1957], classical diffusion theory has found applications as diverse as the propagation of light in clouds [Liou, 1992] and human tissues [Profio, 1989]. In these applications, scattering is often isotropic (e.g., neutron scattering by heavy nuclei), or absorption is negligible (e.g., within clouds) even though the scattering is anisotropic. In sea ice, absorption is often small but not negligible, and scattering is highly anisotropic. Thus sea ice may lie near the boundary where diffusion theory is or is not applicable. We therefore need to examine the extent to which diffusion theory can be used to model light propagation in sea ice. In particular, we want to determine whether or not diffusion theory can be used as a framework for deducing ice scattering properties from measurements of absorption and irradiance.

We first review the possible values for the absorbing and scattering properties of sea ice, and we then review various results from diffusion theory, as are needed in our study. We then examine the use of diffusion theory as a basis for recovering the scattering properties of sea ice. Finally, we investigate the accuracy of diffusion theory near air-ice and ice-water boundaries.

2. Ice Inherent Optical Properties

Because our interest here lies in the general application of diffusion theory to light propagation in sea ice, rather than in the detailed modeling of a particular ice sheet, we assume the ice sheet to be a homogeneous layer bounded above by air and below by sea water. The sky radiance distribution incident onto the ice is assumed known. The air-ice surface can be either smooth or rough. The

inherent optical properties (IOPs) of the ice and water are specified by the absorption coefficient a, scattering coefficient b, and scattering phase function $\tilde{\beta}(\psi)$, where ψ is the scattering angle. For the sea ice, we assume that the phase function can be approximated by a one-term Henyey-Greenstein phase function,

$$\tilde{\beta}(\psi) = \frac{1}{4\pi} \frac{1 - g^2}{(1 + g^2 - 2g\cos\psi)^{3/2}}, \quad (1)$$

where g is the average cosine of the scattering angle,

$$g = 2\pi \int_0^{\pi} \tilde{\beta}(\psi) \cos\psi \sin\psi \, d\psi .$$

With the use of Eq. (1) for $\tilde{\beta}(\psi)$, we can completely specify the ice IOPs via the absorption coefficient a, the mean cosine g, and the albedo of single scattering ω_o, where

$$\omega_o = \frac{b}{a+b} = \frac{b}{c},$$

and $c = a + b$ is the beam attenuation coefficient. The IOPs of the water below the ice are specified in the same way, except that we use a typical ocean-water phase function [*Mobley et al.*, 1993] for $\tilde{\beta}(\psi)$; this phase function has g ≈ 0.93.

Values of the absorption coefficient for sea ice depend strongly on wavelength and range from $a \approx 0.04$ m^{-1} near 470 nm to 0.5 m^{-1} at 700 nm [*Grenfell and Perovich*, 1981]. The scattering coefficient is only weakly dependent on wavelength, but depends strongly on the ice temperature. Values of b are estimated [*Perovich and Grenfell*, 1982] to range from as low as ~10 m^{-1} in melting ice to greater than 400 m^{-1} in very cold ice with precipitated salts present in the brine pockets. Thus, depending on wavelength and environmental conditions, sea ice can have albedos of single scattering in the visible spectrum from as low as $\omega_o \approx 0.95$ (melting ice, red wavelengths) to as large as 0.9999 (very cold ice, blue wavelengths). Predicted g values range from 0.96 (many air bubbles) to 0.99 (few air bubbles) [*Mobley et al.*, submitted]. Such large g values are consistent with scattering in ice being due primarily to diffraction by brine pockets and air bubbles that are much larger than the wavelength of visible light. Measurements on laboratory-grown saline ice [*Grenfell and Hedrick*, 1983] indicate that g may be smaller. However, in those measurements, multiple scattering within the ice samples may have given apparent g values that were smaller than the true (single-scattering) g.

A recent study [*Mobley et al.*, submitted] of the physical and optical properties of sea ice near Barrow, Alaska found that the particular ice sheet under investigation had $a \approx 0.4$ m^{-1} and $b \approx 200$ m^{-1} at a wavelength of 670 nm; thus $\omega_o \approx 0.998$. The Barrow ice was $z_{ice} \approx 1.75$ m thick, which corresponds to an optical depth of $\tau_{ice} = cz_{ice} \approx 350$ at this wavelength. The absorption coefficient was measured from melted ice cores, and the scattering coefficient and mean cosine $g \approx 0.98$ were

computed from modified Mie scattering calculations based on measured size distributions of brine pockets and air bubbles. These IOPs gave good agreement between predicted and measured values of beam spread within the ice interior. After incorporation of a transition layer near the ice surface and of an algal layer at the ice bottom, these IOPs also gave good agreement with the measured reflectance and transmittance of the ice sheet. The Barrow IOP data fall in the mid-range of possible values for sea ice, and we therefore use these values to illustrate various points below.

For a given set of ice IOPs, we can impose various external environmental conditions. In our simulations we considered the extreme cases of sky condition, surface roughness, and water IOPs defined by

- a uniform incident sky radiance vs. a black sky with the sun at a zenith angle of 60°
- a smooth air-ice surface vs. a rough surface
- highly absorbing water ($\omega_o = 0.3$) vs. highly scattering water ($\omega_o = 0.9$)

Any situation occurring in nature should fall within these extreme cases.

3. Diffusion Theory

The fundamental assumption of first-order photon diffusion theory [e.g., *Ishimaru*, 1978] is that the radiance distribution within the medium can be adequately approximated by retaining only the first two terms of its exact expansion in spherical harmonics. In this case, the radiance at any location has a directional distribution given by

$$L_{dif}(\hat{s}) = \frac{1}{4\pi}\left[E_o + 3\vec{E}\cdot\hat{s}\right], \tag{2}$$

where $E_o = \int_{4\pi} L(\hat{s})\, d\Omega(\hat{s})$ is the scalar irradiance, $\vec{E} = \int_{4\pi} L(\hat{s})\, \hat{s}\, d\Omega(\hat{s})$ is the vector irradiance, $\hat{s}$ is a unit vector specifying the polar (θ) and azimuthal (ϕ) directions in some convenient coordinate system, and $d\Omega(\hat{s}) = \sin\theta\, d\theta\, d\phi$ is the differential element of solid angle.

Integrating the source-free radiative transfer equation (RTE),

$$\hat{s}\cdot\nabla L(\hat{s}) = -cL(\hat{s}) + b\int_{4\pi} L(\hat{s}')\, \tilde{\beta}(\hat{s}'\rightarrow\hat{s})\, d\Omega(\hat{s}'),$$

over all directions gives the divergence law for irradiance (Gershun's equation),

$$\nabla\cdot\vec{E} = -aE_o. \tag{3}$$

Inserting the radiance distribution of Eq. (2) into the RTE, multiplying by $\hat{s}$, integrating over all directions, and considering only locations far from a boundary gives Fick's law [*Ishimaru*, 1978; see also *Maffione*, in press, for a discussion of the subtleties of this derivation],

$$\vec{E} = -D\nabla E_o , \tag{4}$$

where

$$D = \frac{1}{3c(1 - g\omega_o)} . \tag{5}$$

In the present study we are assuming the IOPs to be independent of position; therefore D is a constant. Inserting (4) into (3) then gives

$$\nabla^2 E_o = \frac{a}{D} E_o , \tag{6}$$

which is recognized as a first-order diffusion equation for the scalar irradiance, with D being the diffusion coefficient.

We restrict ourselves to a plane-parallel geometry with depth z as the only spatial variable, as is appropriate for our study of sea ice; θ is measured from the nadir direction. In this case, the one-dimensional form of Eq. (6),

$$\frac{d^2 E_o(z)}{dz^2} = \frac{a}{D} E_o(z) ,$$

has the solution

$$E_o(z) = E_o(0)\, e^{-\kappa z} , \tag{7}$$

where

$$\kappa = \sqrt{\frac{a}{D}} \tag{8}$$

is the decay rate with depth of the scalar irradiance.

In our one-dimensional geometry, $\vec{E}\cdot\hat{s} = E\cos\theta$, where E is the net vertical irradiance ($= E_d - E_u$, where E_d and E_u are respectively the downwelling and upwelling plane irradiances). Equations (4) and (7) then allow us to write the diffusion-theory radiance of Eq. (2) as

$$L_{dif}(z,\theta) = \frac{E_o(0)}{4\pi}\left[1 + 3\kappa D\cos\theta\right] e^{-\kappa z} . \tag{9}$$

Note that this radiance, and hence every radiometric quantity, decays with depth at the rate given by κ, which can be written as

$$\kappa = c\sqrt{3(1 - \omega_o)(1 - g\omega_o)} . \tag{10}$$

Relations (5), (8) and (10) between D, κ, and the IOPs are independent of the exact form of the scattering phase function; phase function information enters diffusion theory only via the mean cosine of the scattering angle, g.

4. Recovery of Ice Scattering Properties

Our primary interest in diffusion theory lies in its use as a theoretical framework for deducing the scattering properties of sea ice, which are exceptionally difficult to measure. If accurate estimates of b and g can be obtained, then those values can be combined with measured or modeled values of a and used as input to sophisticated radiative transfer models which, unlike diffusion theory, provide an exact description of the light field.

Equation (10) provides an important constraint on the possible values of g. We noted in Section 2 that the Barrow ice sheet had $a \approx 0.4$ m^{-1} and $b \approx 200$ m^{-1}, so that $\omega_o \approx 0.998$, and that the ice was optically very thick. Because of this high ω_o value, we can reasonably assume that diffusion theory is valid in the interior of the Barrow ice. The measured decay rate of the downwelling irradiance for the Barrow ice sheet was $K_d \approx 2.3$ m^{-1} (averaged over the entire thickness of the ice). This K_d corresponds to κ in the framework of diffusion theory. Solving Eq. (10) for g and using K_d for κ gives

$$g = 1 - \frac{1}{b}\left(\frac{K_d^2 - 3a^2}{3a}\right). \tag{11}$$

Substituting the values just cited for a, b, and K_d gives $g \approx 0.98$, which is consistent with the g value computed in *Mobley et al.* [submitted] using Mie theory and measured ice physical properties. This result provides an important check on those calculations, which required a number of assumptions in applying Mie theory to the non-spherical brine pockets.

If we exclude melting ice, b values are generally greater than 100 m^{-1}. For a wide variety of ice types, K_d values are in the range of 1 to 5 m^{-1} at visible wavelengths [*Grenfell and Maykut*, 1977] and a is generally less than 0.5 m^{-1}. These K_d values correlate with the a values, e.g. both are smallest at blue wavelengths and largest at red wavelengths. Equation (11) then constrains g to be generally greater than 0.9, and often very near 1, as is the case for the Barrow ice. This constraint on g suggests that the laboratory measurements of *Grenfell and Hedrick* [1983], which gave g's as low as 0.6, were indeed contaminated by multiple scattering.

Values of g very near one greatly restrict the range of ω_o values for which diffusion theory is valid. Figure 1 shows how quickly diffusion theory departs from reality when the scattering phase function is highly anisotropic. The figure compares the exact asymptotic radiance distribution L_∞ computed using an eigenmatrix method [*Mobley*, 1994, Section 9.6] with the diffusion solution L_{dif} of Eq.(9). The phase function of Eq. (1) with $g = 0.98$ was used in the eigenmatrix calculations. When there is no absorption, $\omega_o = 1$, the asymptotic radiance distribution is isotropic and the diffusion solution is exact. The agreement between L_∞ and L_{dif} is still quite good at $\omega_o = 0.999$. However, at $\omega_o = 0.99$ there is a considerable difference in L_∞ and L_{dif}, and L_{dif} has even become negative at $\theta = 180°$. Equation (9) shows that L_{dif} becomes negative at large θ if $3\kappa D > 1$, which

occurs when $\omega_o < 2/(3 - g)$, or 0.9901 in the present case. This situation can be contrasted to that for isotropic scattering, $g = 0$, for which L_{dif} would not become negative until ω_o decreased to 2/3.

The absorption coefficient a of sea ice can be measured by extracting and melting ice cores and then using standard instruments and techniques to measure the absorption of the meltwater. The depth-averaged attenuation rate K_d of an ice sheet is routinely determined from measurements of the downwelling plane irradiances just above and below the ice; this is what was done for the Barrow ice. Depth profiles of the irradiance within the ice are also sometimes measured by drilling horizontal holes into the wall of an ice pit and inserting a cosine collector into the hole far enough to be away from the boundary effects of the ice pit. Such measurements can give an even better estimate of κ in the interior of the ice. In any case, we assume that the absorption coefficient a and the diffuse attenuation κ are known.

Equation (11) gives a relation between the scattering parameters b and g and the known a and κ. If we can obtain another equation relating b and g to measurable quantities, we can then simultaneously solve that equation along with Eq. (11) to obtain both b and g. One way to add information to a and κ is to make additional measurements. Suppose, for example, that we measure the irradiance reflectance $R = E_u/E_d$ in the center of the ice layer, where diffusion theory is most accurate. Such measurements could be made within the same horizontal holes mentioned above in the measurement of downwelling irradiances within the ice. The same instrument could be turned upside down to obtain E_u.

Integration of L_{dif} shows that, according to diffusion theory,

$$R = \frac{1 - 2\kappa D}{1 + 2\kappa D},$$

which can be rewritten as

$$b(1 - g) = a\left[\frac{4}{3}\left(\frac{1 + R}{1 - R}\right)^2 - 1\right]. \tag{12}$$

It might be supposed that Eqs. (11) and (12) now give us the desired two equations in b and g, assuming that a, κ and R are known. Unfortunately, this is not the case: note that b and g appear only as the product $b(1\text{-}g)$ in both equations. Physically, once a and κ are determined, so is κD, the radiance, and hence every apparent optical property. Thus, in the context of diffusion theory, no measurement of an apparent optical property such as the reflectance can add additional information to that already available in a and κ, and we are thwarted in our attempt to recover both b and g.

If both b and g are to be recovered, then an additional measurement of an inherent optical property (such as the beam attenuation c) must be made, or the inversion algorithm must be based on a more sophisticated model of light propagation than is given by diffusion theory. For example, *Maffione and Mobley* [in press] have shown how to measure the complete beam spread function (BSF) along horizontal paths within ice. The development of the BSF with path length and direction

is sensitive to b and g (and far beyond the simplicity of diffusion theory). Thus BSF measurements do provide additional information, which may be sufficient to yield both b and g from a suitable inversion algorithm. The idea of inverting the sea ice BSFs is not new [*Tanis*, 1994], but previous inversion algorithms have been applied to only to BSFs measured over a limited angular range in the paraxial approximation. The measurement method described in *Maffione and Mobley* [in press] gives BSFs over the full angular range, and therefore inversion algorithms may provide better results than before. Such inversions of sea ice BSFs warrant further investigation.

5. Boundary Effects

The radiance distribution of Eq. (9) cannot satisfy boundary conditions for the incident radiance at the ice surface [*Ishimaru*, 1978]. Therefore, diffusion theory can describe the light field only when sufficiently far from boundaries, i.e. in the asymptotic regime discussed in Fig. 1. How far one must be from a boundary and how large ω_0 must be depends both on the IOPs and on the accuracy required from the diffusion approximation. However, convenient rules [*Zega et al.*, 1991, p. 75] suggest that diffusion theory can be used in semi-infinite, plane parallel geometry when the optical depth, τ, and ω_0 satisfy

$$\tau > \frac{4}{3(1 - g)} \quad \text{and} \quad \omega_0 > 1 - 0.3(1 - g). \tag{13}$$

For $g = 0.98$, as for the Barrow ice, these conditions require $\tau > 67$ and $\omega_0 > 0.994$. Thus, as we assumed in the previous section, diffusion theory should give a good description of the light field in the interior of the Barrow ice layer, which had an optical thickness of $\tau \approx 350$. The large values of τ and ω_0 required for the application of diffusion theory to sea ice can again be contrasted with the values of $\tau \geq 4/3$ and $\omega_0 \geq 0.7$ that satisfy Eq. (13) when scattering is isotropic.

In order to investigate the magnitude of boundary effects on the light field in sea ice, we next used the Hydrolight radiative transfer numerical model [*Mobley*, 1994] to compute the exact radiance distribution throughout an ice sheet with IOPs corresponding to the Barrow data. The simulation used a cardioidal radiance distribution,

$$L_{\text{card}}(\theta) = \frac{E_{\text{od}}}{4\pi}[1 + 2\cos\theta], \quad 0 \leq \theta \leq \frac{\pi}{2}, \tag{14}$$

to define the angular pattern of the sky radiance incident onto the ice surface; the downwelling sky scalar irradiance E_{od} was set to 1 W m^{-2} nm^{-1}. The cardioidal distribution is a good approximation of the sky radiance for a heavily overcast sky, as often occurs in the Arctic. The air-ice surface was taken to be rough. The water was taken to be moderately scattering, $\omega_0 = 0.7$, and infinitely deep below the ice layer.

Figure 2 shows the exact and diffusion radiance distributions just below the air-ice surface ($\tau = 0$), at the mid-depth of the ice layer ($\tau = 175$), and at the bottom of the ice ($\tau = 350$). At each depth the diffusion curve is normalized to the value of $L(\theta=0)$ for ease in comparing the shapes of the curves; the actual value of L_{dif} given by Eq. (9) also is offset in magnitude from the exact L because the diffusion value for E_o, as given by Eq. (7), differs from the exact value (see Fig. 3 below). As expected, the radiance distribution near the ice surface differs greatly in shape from the diffusion solution because of the proximity of the boundary. This difference is can be much larger for other boundary conditions, such as a bright sun in a clear sky.

Beginning a few tens of optical depths below the surface, the diffusion solution provides a good approximation to the actual radiance. This agreement, which is shown in Fig. 2 only at the mid-depth, holds until within a few tens of optical depths from the ice-water boundary. L and L_{dif} then again begin to differ as the radiance in the ice starts to feel the effect of the discontinuity in the IOPs at the ice-water boundary. Thus, consistent with Eq. (13), L_{dif} proves to be a good approximation of the exact radiance distribution only in the ice interior, which is 50 τ 300 in the present example.

The bottom set of curves in Fig. 2 shows that the radiance distribution exiting the bottom of the ice into the water (i.e., for $0 \le \theta \le 90°$) is noticeably different from L_{dif}. The dotted line for the bottom group of curves shows the normalized cardioidal distribution of Eq. (14). The cardioidal distribution is seen to give a very good approximation to the exact radiance exiting the ice into the water, except for nearly horizontal ($\theta \approx 90°$) directions. This is not surprising because an ice-to-water transition is similar to a stratus-cloud-to-clear-air transition, which is the historical origin of the empirically determined cardioidal distribution. This analogy is reasonable at the ice-water boundary, where there is a large change in the scattering properties but little change in the real index of refraction, which is almost the same for ice and water. Thus, just as at the bottom of a cloud, there is little internal reflection or refraction at the ice bottom. At the air-ice surface there is a large change in both the scattering properties and the index of refraction; and internal reflection within the ice and refraction across the surface explain, at least in part, why the cardioidal distribution gives a poor approximation of the radiance exiting the ice into the air. We note in passing that the cardioidal distribution cannot represent a solution of the diffusion equation in spite of the superficial similarity of Eqs. (9) and (14) in their θ dependence. This is because $3\kappa D$ can never equal 2; for the Barrow IOPs, $3\kappa D \approx 0.5227$ and so L_{dif} is considerably different from L_{card}.

Figure 3 shows the depth dependence of the exact and diffusion scalar irradiances E_o. The profile of E_o as predicted by diffusion theory is obtained from Eq. (7) assuming that $E_o(0)$ is known exactly, even though diffusion theory provides no way to determine $E_o(0)$. In these simulations, the value of $E_o(0) = 2.05$ W m^{-2} nm^{-1} was obtained from the Hydrolight numerical solution. Note that it is correct that $E_o(0)$ is greater than the value of E_{od}(air) = 1 W m^{-2} nm^{-1}: $E_o(0)$ includes contributions from that part of E_{od}(air) that is transmitted through the air-ice surface, from the

upwelling light within the ice, and from the upwelling light that is reflected back downward by the air-ice surface.

Because of optical boundary effects, diffusion theory generally underestimates the scalar irradiance E_o near the surface of the ice and overestimates it near the bottom. Thus the same behavior is seen in the magnitudes of L_{dif} and other irradiances. This qualitative behavior holds true for the full range of sky conditions, surface roughness, water IOPs, and ice IOPs considered in our simulations. In the present case, diffusion theory gives a value of E_o at the bottom of the ice that is 4.3 times the correct value. Clearly, diffusion theory cannot be used to predict the scalar irradiance at the very bottom of the ice, $E_o(z_{ice})$, which is a primary input to biological productivity models of ice algae layers. Likewise, diffusion theory should not be used to compute the depth profile of heating, which is proportional to $E_o(z)$, even though our simulations show that the average heating throughout the ice layer often can be predicted to within 10 per cent.

Accurate and efficient numerical models such as Hydrolight, or the models of Grenfell [1991] or Jin et al. [1994], are readily available for the prediction of light propagation in sea ice if the IOPs are given. Unlike diffusion theory, these models properly handle boundary conditions and stratified ice. There is thus little to recommend in the use of diffusion theory for the prediction of light fields within sea ice.

6. Conclusions

Numerical simulations have shown that, as anticipated, diffusion theory gives reasonably accurate predictions of light propagation deep in the interior of thick sea ice layers. However, because of boundary effects, diffusion theory cannot be used to predict irradiances at the bottom of the ice, as are needed for input to biological productivity models, nor can diffusion theory be used to predict the radiance or irradiance exiting an ice sheet into the atmosphere or into the water below. The angular radiance distribution exiting the ice into the water is well approximated by a cardioidal distribution, although the same is not true for the radiance exiting the ice into the atmosphere.

Diffusion theory provides an important constraint on the possible values of the average cosine of the scattering angle, which is a primary input to all radiative transfer models. However, diffusion theory is too simple to provide a theoretical framework for recovery of both the average cosine and the scattering coefficient b. It is not possible to alleviate this problem via additional measurements, because of the highly constrained form of the radiance in diffusion theory. Thus, the scattering properties of sea ice, which are crucial to the accurate modeling of light propagation in ice, must therefore be obtained by other means. For example, it may be possible to invert measurements of beam spread along horizontal paths is sea ice to obtain additional information about sea ice volume scattering functions.

Acknowledgments

Author C.D.M. was supported in this research by the Environmental Optics Program of the Office of Naval Research under contract N00014-97-C-0023. Author R.A.M. was supported by the same program under contract N00014-97-C-0006. The development of Hydrolight has been supported separately by various ONR contracts. This work was conducted as part of the ONR Electromagnetic Properties of Sea Ice Accelerated Research Initiative.

References

Davison, B. and J. B. Sykes, *Neutron Transport Theory*, Oxford Univ. Press, 450 pages, 1957.

Eddington, A. S., On the radiative equilibrium of the stars. *Mon. Not. Roy. Astron. Soc., 77*, 16-35, 1916.

Grenfell, T. C., A radiative transfer model for sea ice with vertical structure variations, *J. Geophys. Res., 96*(C9), 16991-17001, 1991.

Grenfell, T. C. and D. Hedrick, Scattering of visible and near infrared radiation by NaCl ice and glacier ice, *Cold Reg. Sci. Tech., 8*, 119-127, 1983.

Grenfell, T. C. and G. A. Maykut, The optical properties of ice and snow in the Arctic Basin, *J. Glaciol., 18*(80), 445-463, 1977.

Grenfell, T. C. and D. K. Perovich, Radiation absorption coefficients of polycrystalline ice from 400-1400 nm, *J. Geophys. Res., 86*(C8), 7447-7450, 1981.

Ishimaru, A., *Wave Propagation and Scattering in Random Media, Vol. 1, Single Scattering and Transport Theory*, Academic Press, 250 pages, 1978.

Jin, Z., K. Stamnes, W. F. Weeks, and S.-C. Tsay, The effect of sea ice on the solar energy budget in the atmosphere-sea ice-ocean system: A model study, *J. Geophys. Res., 99*(C12), 25281-25294, 1994.

Liou, K. N., *Radiation and Cloud Processes in the Atmosphere: Theory, Observation, and Modeling*, Oxford Univ. Press, 487 pages, 1992.

Maffione, R. A., Theoretical developments on the optical properties of highly turbid waters and sea ice, *Limnol. Oceanogr.*, in press.

Maffione, R. A. and C. D. Mobley, Theory and measurements of the complete beam spread function of sea ice, *Limnol. Oceanogr.*, in press.

Mobley, C. D., *Light and Water: Radiative Transfer in Natural Waters*, Academic Press, 592 pages, 1994.

Mobley, C. D., B. Gentili, H. R. Gordon, Z. Jin, G. W. Kattawar, A. Morel, P. Reinersman, K. Stamnes, and R. H. Stavn, Comparison of numerical models for computing underwater light fields, *Appl. Optics, 32*(36), 7484-7504, 1993.

Mobley, C. D., G. F. Cota, T. C. Grenfell, R. A. Maffione, W. S. Pegau, and D. K. Perovich, Modeling light propagation in sea ice, *IEEE Trans. Geosci. Rem. Sens.*, submitted.

Perovich, D. K. and T. C. Grenfell, A theoretical model of radiative transfer in young sea ice, *J. Glaciol., 18*, 341-357, 1982.

Profio, A. E., Light transport in tissue, *Appl. Optics, 23*(12), 2216-2221, 1989.

Tanis, F. J., Use of beam spreading measurements to estimate volume scattering properties in sea ice, *Ocean Optics XII*, J. S. Jaffe, Editor, Proc. SPIE Vol. 2258, 965-973, 1994.

Zega, E. P., A. P. Ivanov, and I. L. Katsev, *Image Transfer Through a Scattering Medium*, Springer Verlag, 334 pages, 1991.

Figure Captions

Fig. 1. Comparison of the exact asymptotic radiance distribution L_∞ (solid lines) with that given by diffusion theory, L_{dif} (dashed lines). The phase function is that of Eq. (1) with $g = 0.98$.

Fig. 2. Comparison of the exact radiances (solid lines) with the corresponding radiances given by diffusion theory (normalized to the exact values at $\theta = 0$; dashed lines). The ice IOPs are those of the Barrow ice; the optical depth of $\tau = 350$ is the ice-water boundary at $z_{ice} = 1.75$ m.

Fig. 3. The exact depth profile of E_0 (solid line) and the corresponding profile within the ice as given by diffusion theory (dashed line). All IOPs and environmental conditions are the same as for Fig. 2.

prog: pfig1
file: linfg98.dat

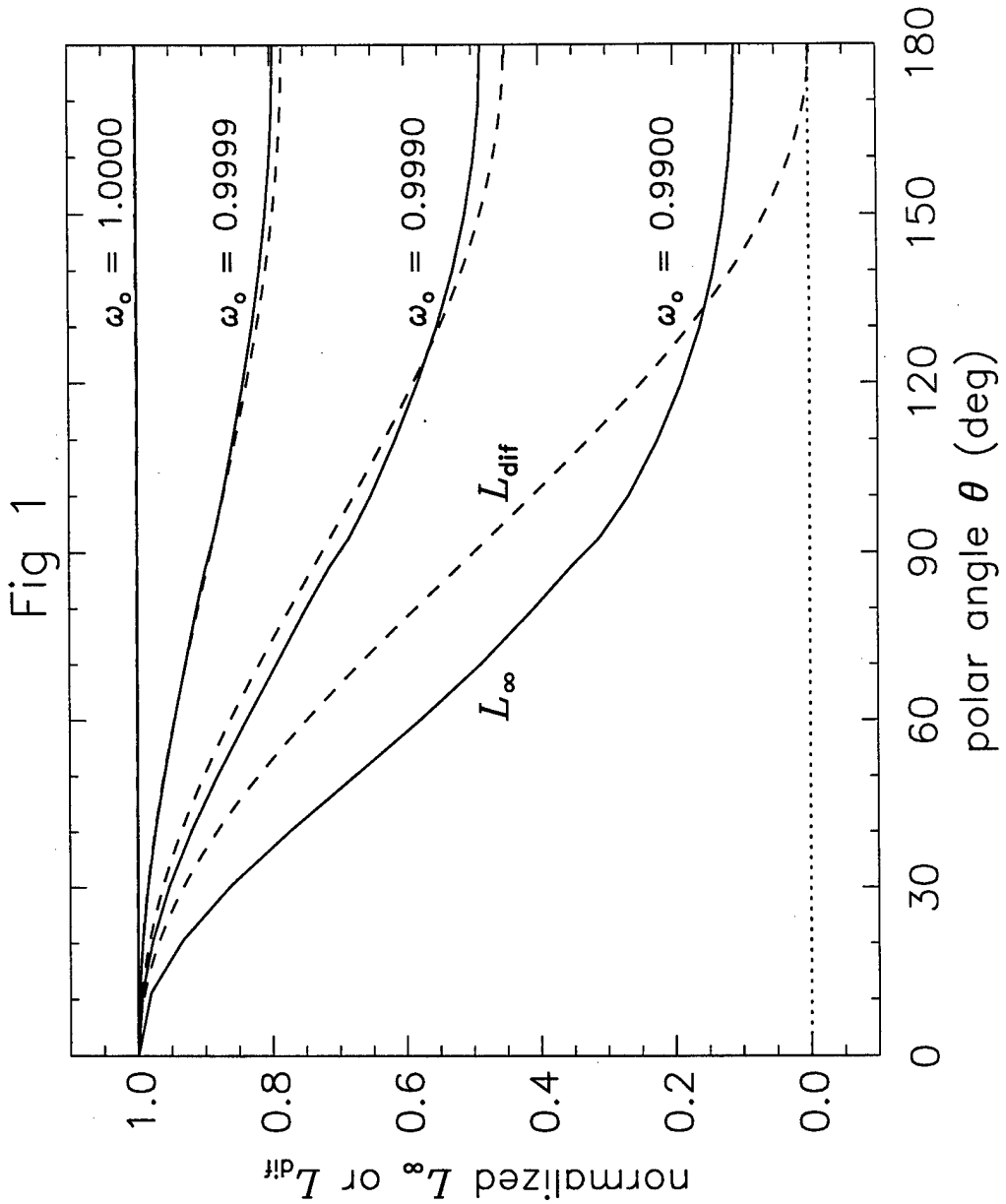

prog: pfig2
file: ../archive/raddiff.f2

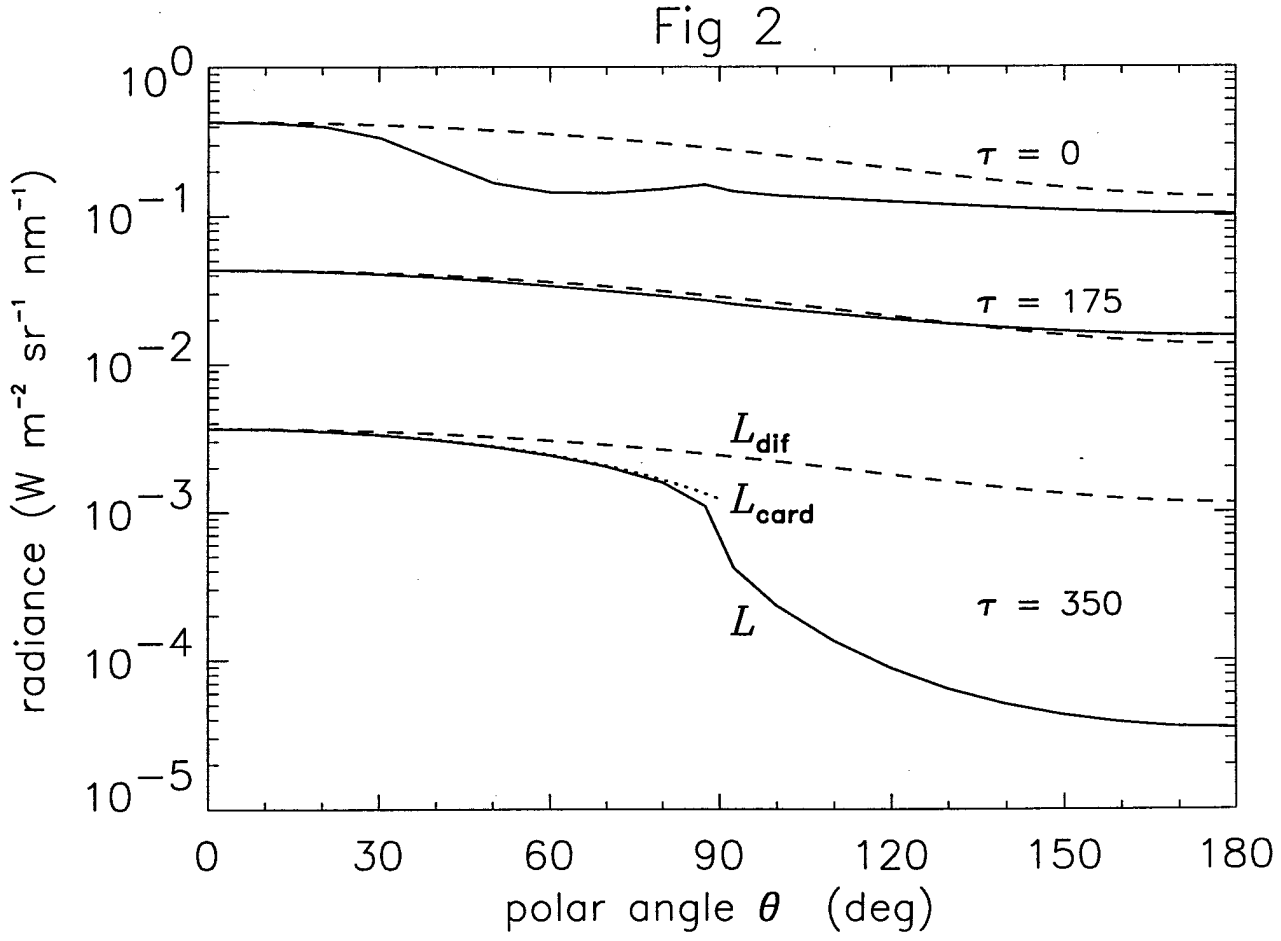

prog: pfig3
file: ../archive/raddiff.f2

Fig. 3